



New Cases of Superflares on Slowly Rotating Solar-type Stars and Large Amplitude Superflares in G- and M-type Main Sequence Stars

A. K. Althukair^{1,2}  and D. Tsiklauri¹ 

¹ Department of Physics and Astronomy, School of Physical and Chemical Sciences, Queen Mary University of London, Mile End Road, London, E1 4NS, UK
a.k.althukair@qmul.ac.uk, d.tsiklauri@qmul.ac.uk

² Physics Department, College of Sciences, Princess Nourah Bint Abdulrahman University, Riyadh, P.O. Box 84428, Saudi Arabia
Received 2023 June 3; revised 2023 July 8; accepted 2023 July 25; published 2023 September 20

Abstract

In our previous work, we searched for superflares on different types of stars while focusing on G-type dwarfs using entire Kepler data to study statistical properties of the occurrence rate of superflares. Using these new data, as a by-product, we found 14 cases of superflare detection on 13 slowly rotating Sun-like stars with rotation periods of 24.5–44 days. This result supports the earlier conclusion by others that the Sun may possibly undergo a surprise superflare. Moreover, we found 12 and seven new cases of detection of exceptionally large amplitude superflares on six and four main sequence stars of G- and M-type, respectively. No large-amplitude flares were detected in A, F or K main sequence stars. Here we present preliminary analysis of these cases. The superflare detection, i.e., an estimation of flare energy, is based on a more accurate method compared to previous studies. We fit an exponential decay function to flare light curves and study the relation between e-folding decay time, τ , versus flare amplitude and flare energy. We find that for slowly rotating Sun-like stars, large values of τ correspond to small flare energies and small values of τ correspond to high flare energies considered. Similarly, τ is large for small flare amplitudes and τ is small for large amplitudes considered. However, there is no clear relation between these parameters for large amplitude superflares in the main sequence G- and M-type stars, as we could not establish clear functional dependence between the parameters via standard fitting algorithms.

Key words: stars: activity – stars: flare – stars: rotation – stars: solar-type – stars: statistics – Sun: flares

1. Introduction

It is believed that solar and stellar flares are powered by a physical process called magnetic reconnection, in which connectivity of magnetic field lines in the atmospheres of stars changes rapidly (Masuda et al. 1994; Shibata et al. 1995). This is accompanied by acceleration of plasma particles and release of heat. The source of this kinetic and thermal energy is the energy stored in the magnetic field. Thus, the magnetic dynamo process which is one possible means to generate a magnetic field via bulk plasma flows is of great importance for understanding what can power and therefore be the source for a flare or a superflare. The energies of observed stellar flares lie in a wide range from 10^{28} to 10^{37} erg, while the highest energy of any observed solar flare is approximately a few times 10^{32} erg. Thus, generally agreed terminology is that a superflare should have an energy in excess of 10^{34} erg. A plausible dynamo model capable of explaining the generation of magnetic energy sufficient to support superflares has been recently suggested in Kitchatinov & Olemskoy (2016) and then further investigated in Katsova et al. (2018). In this scenario, rather than producing stellar cycles similar to the solar 11 yr cycle, the dynamos in superflaring stars excite some quasi-stationary magnetic configuration with a much higher magnetic

energy. Further, Kitchatinov et al. (2018) used a flux-transport model for the solar dynamo with fluctuations of the Babcock-Leighton type α -effect to generate statistics of magnetic cycles. As a result, they concluded that the statistics of the computed energies of the cycles suggest that superflares with energies in excess of 10^{34} erg are not possible on the Sun.

Historical records suggest that no superflares have occurred on the Sun in the last two millennia. In the past there were notable examples of detection of superflares on Sun-like stars. There are two references which support such claim: Schaefer et al. (2000) and Nogami et al. (2014).

As asserted by Schaefer et al. (2000), nine cases of superflares were identified involving 10^{33} to 10^{38} erg on main sequence Sun-like stars. Sun-like means that stars are on or near the main sequence, have spectral class from F8 to G8 and are single (or have a very distant binary companion). The superflare energy estimation by Schaefer et al. (2000) was based on photometric methods.

Nogami et al. (2014) reported the results of high dispersion spectroscopy of two “superflare stars,” KIC9766237 and KIC9944137, using the Subaru/HDS telescope. These two stars are G-type main sequence stars, and have rotation periods of 21.8 days and 25.3 days, respectively. Their spectroscopic

results confirmed that these stars have stellar parameters similar to those of the Sun in terms of the effective temperature, surface gravity and metallicity. By examining the absorption line of Ca II 8542, the average strength of the magnetic field on the surface of these stars was estimated to be 1–20 G. The superflare energy estimation by Nogami et al. (2014) was based on a semi-empirical method considering magnetic energy density times volume of flare. These results claim that the spectroscopic properties of these superflare stars are very close to those of the Sun, and support the hypothesis that the Sun may have a superflare. What causes superflares is an open issue and many theories exist to explain their origin. Karak et al. (2020) demonstrated that Sun-like slowly rotating stars, having antisolar differential rotation (DR), i.e., when equatorial regions of the star rotate slower than the polar regions, can produce a very strong magnetic field and that could be a possible explanation for a superflare. It is the antisolar DR that can produce strong fields in slowly rotating stars. A study conducted by Karak et al. (2020) focused on mean-field kinematic dynamo modeling to investigate the behavior of large-scale magnetic fields in different stars with varying rotation periods. They specifically consider two cases: stars with rotation periods larger than 30 days, which exhibit antisolar DR, and stars with rotation periods shorter than 30 days, which manifest solar-like DR. The study supports the possible existence of antisolar DR in slowly rotating stars and suggests that these stars may exhibit unusually enhanced magnetic fields and potentially produce cycles that are prone to the occurrence of superflares. In general the transition from solar to antisolar DR happens somewhere around the Rossby number of unity. For the Sun, it is obviously solar-like, but when the rotation rate decreases, one expects to have an antisolar DR. This robust transition has been seen in many numerical simulations. Karak et al. (2015), for example, using global magnetohydrodynamics (MHD) convection simulations, consistently find antisolar DR when the star rotates slowly.

Statistical study of superflares on different stellar types has been an active area of research (Maehara et al. 2012; Shibayama et al. 2013; He et al. 2015, 2018; Wu et al. 2015; Van Doorselaere et al. 2017; Yang et al. 2017; Lu et al. 2019; Yang & Liu 2019; Günther et al. 2020; Tu et al. 2020; Gao et al. 2022). Shibayama et al. (2013) examined statistics of stellar superflares. These authors discovered that for Sun-like stars (with surface temperature 5600–6000 K and slowly rotating with periods longer than 10 days), the occurrence rate of superflares with an energy of 10^{34} – 10^{35} erg is once in 800–5000 yr. Shibayama et al. (2013) confirmed the previous results of Maehara et al. (2012) in that the occurrence rate (dN/dE) of superflares versus flare energy E shows a power-law distribution with $dN/dE \propto E^{-\alpha}$, where $\alpha \sim 2$. Such occurrence rate distribution versus flare energy is roughly similar to that for solar flares. Tu et al. (2020) identified and verified 1216 superflares on 400 solar-type stars by analyzing 2

minute cadence data from 25,734 stars observed during the first year of the Transiting Exoplanet Survey Satellite (TESS) mission. The results indicate a higher frequency distribution of superflares compared to the findings from the Kepler mission. This difference may be due to a significant portion of TESS solar-type stars in the data set that are rapidly rotating. The power-law index γ of the superflare frequency distribution was determined to be $\gamma = 2.16 \pm 0.10$, which is consistent with the results obtained from the Kepler mission. The study highlights an extraordinary star, TIC 43472154, which exhibits approximately 200 superflares per year. Tu et al. (2020) analyzed the correlation between the energy and duration of superflares, represented as $T_{\text{duration}} \propto E^{\beta}$. They derived a power-law index $\beta = 0.42 \pm 0.01$ for this correlation, which is slightly larger than the value of $\beta = 1/3$ predicted by magnetic reconnection theory. A similar conclusion had been reached earlier by Maehara et al. (2015), who found that the duration of superflares, τ , scales as the flare energy, E , according to $\tau \propto E^{0.39 \pm 0.03}$. Yang et al. (2023) analyzed TESS light curves from the first 30 sectors of TESS data with a two-minute exposure time. They identified a total of 60,810 flare events occurring on 13,478 stars and performed a comprehensive statistical analysis focusing on the characteristics of flare events, including their amplitude, duration and energy. We believe that the method for flare energy estimation used in Shibayama et al. (2013); Yang et al. (2017) is more accurate than the one used by Schaefer et al. (2000) and Nogami et al. (2014). We therefore base the flare energy estimate on the method of Shibayama et al. (2013) and Althukair & Tsiklauri (2023), referred to hereafter as Paper I.

In Paper I we searched for superflares on different spectral classes stars, while focusing on G-type dwarfs (solar-type stars) using Kepler data from quarter (Q) Q0–Q17 with the purpose of examining the statistical properties of the occurrence rate of superflares. Shibayama et al. (2013) considered statistics of stellar superflares based on Kepler data in Q0–Q6. In Paper I we investigated how the results were modified by adding more quarters, i.e., what is the α power-law for data from Q0–Q17 and Q7–Q17. Here using the more extended Kepler data, we also found 14 cases of detection of superflares on 13 slowly rotating Sun-like stars in each of KIC 3124010, KIC 3968932, KIC 7459381, KIC 7668358, KIC 7821531, KIC 9142489, KIC 9528212, KIC 9963105, KIC 10275962, KIC 11086906, KIC 11199277, KIC 11350663 and KIC 11971032. Thus the main purpose of the present study is to present analysis of these new 14 cases. The main novelty here is that the detection is based on the Shibayama et al. (2013) method, which is more accurate, as compared to Schaefer et al. (2000) and Nogami et al. (2014) for the flare energy estimation. Our results support the earlier conclusion by others (Schaefer et al. 2000 and Nogami et al. 2014) that the Sun may have a surprise superflare. We stress that Paper I has conducted a more comprehensive study of determination of stellar rotation

periods based on a robust method such as utilized by McQuillan et al. (2014) in comparison to Shibayama et al. (2013). We believe that more accurate period determination used in Paper I has led to the current new results, presented in this paper. In addition to the 14 cases of superflares on slowly rotating Sun-like stars, we detected 12 and seven superflares with a large amplitude on five G-type and four M-type main sequence stars, respectively.

Solar flares emit energy at all wavelengths, but their spectral distribution is still unknown. When white-light continuum emission is observed, the flares are referred to as “white-light flares” (WLFs). Kretzschmar (2011) identified and examined visible light emitted by solar flares and found that the white light is present on average during all flares and must be regarded as continuum emission. Kretzschmar (2011) also demonstrated that this emission is consistent with a blackbody spectrum with temperature of 9000 K and that the energy of the continuum contains roughly 70% of the total energy emitted by the flares. WLFs are among the most intense solar flares, and it has been demonstrated that an optical continuum appears anytime the flare’s extreme-ultraviolet (EUV) or soft X-ray luminosity reaches a reasonably large threshold (McIntosh & Donnelly 1972; Neidig & Cliver 1983). Thus, optical continuum is presumably present in all flares but only in a few cases does it reach a measurable degree of brightness. This conclusion implies that WLFs are not fundamentally different from conventional flares (Neidig 1989). Nonetheless, WLFs are important in flare studies because they are similar to stellar flares (Worden 1983) and because they represent the most extreme conditions encountered in solar optical flares (Neidig 1989). Considering observations from TESS, Ilin et al. (2021) present four fully convective stars that exhibited WLFs with large size and long duration. The underlying flare amplitude as a fraction of the quiescent flux of two flares is greater than two. After the discovery of the largest amplitude flares ever recorded on an L0 dwarf, which reached $\Delta V \approx -11$ magnitude, Schmidt et al. (2016); Jackman et al. (2019) detected a large amplitude white-light superflare on the L2.5 dwarf ULAS J224940.13011236.9 with flux $\Delta V \approx -10$ magnitude which corresponds to a relative brightness ratio of 10,000. This can be demonstrated as follows

$$\Delta V = V_{\max} - V_{\min} \approx -10, \quad (1)$$

where V_{\max} is the apparent magnitude in the visible band corresponding to the flux at the maximum amplitude F_{\max} , and V_{\min} is the apparent magnitude in the visible band corresponding to the flux at the minimum state F_{\min} . Using the magnitude difference calculation

$$V_{\max} - V_{\min} = -10 = 2.5 \log_{10}(F_{\min}/F_{\max}), \quad (2)$$

it is clear that $F_{\max}/F_{\min} = \Delta F/F = 10000$.

Stellar superflares have been studied in multiple wavelength bands, such as X-rays and the $H\alpha$ band. It is important to mention relevant studies here: Wu et al. (2022) analyzed

spectroscopic data from LAMOST Data Release 7 (DR7) and identified a stellar flare on an M4-type star that is characterized by an impulsive increase followed by a gradual decrease in the $H\alpha$ line intensity. The $H\alpha$ line, which corresponds to a specific transition in hydrogen, exhibited a Voigt profile during the flare. After the impulsive increase in the $H\alpha$ line intensity, a clear enhancement was observed in the red wing of the $H\alpha$ line profile. Additionally, the estimated total energy radiated through the $H\alpha$ line during the flare is on the order of 10^{33} erg, providing an indication of the overall energy release associated with the event. Chandra/HETGS time-resolved X-ray spectroscopic observations were used by Chen et al. (2022) to study the behavior of stellar flares on EV Lac. They discovered distinct plasma flows caused by flares in the corona of EV Lac, but none of them provided evidence for the actual occurrence of stellar coronal mass ejections (CMEs). In most flares, the flow of plasma is accompanied by a rise in the density and temperature of the coronal plasma.

Here we present the detection of 14 superflares on 13 slowly rotating Sun-like stars, 12 and seven cases of large amplitude superflares on five G-type dwarfs and four M-type dwarfs respectively. Section 2 presents the method used including the flare detection, flare energy estimation and rotation period determination. Section 3 reports the main results of this study. Section 4 closes this work by providing our main conclusions.

2. Methods

2.1. Flare Detection

We conducted an automated search for superflares on main sequence star types A, F, G, K and M based on the entire Kepler data, using our Python script for long cadence data from Data Release 25 (DR25) following the Maehara et al. (2012); Shibayama et al. (2013) method. The parameters for all targets observed by Kepler have been taken from the Kepler Stellar interactive table in the NASA Exoplanet Archive. The study was carried out on a sample of main sequence stars, comprising 2222, 10,307, 25,442, 10,898 and 2653 stars with spectral types of M, K, G, F and A, respectively. The following is a brief description of this method. We generate light curves of the stars using the PDCSAP flux. Then, in order to be statistically precise, we computed the distributions of brightness variation by calculating the flux difference in adjacent time intervals between every two neighboring data points in the light curve. Then, we determine the flux difference value at which the area under the distribution equals 1% of the total area. In order to increase the threshold, the 1% value of the area was multiplied by a factor of three. The start time of a flare was defined as the time at which the flux difference between two consecutive points exceeded the threshold for the first time. To determine the end time of the flare, we computed the three standard deviations, 3σ , for the distribution of brightness variation. Figure 1 displays typical results for this method for

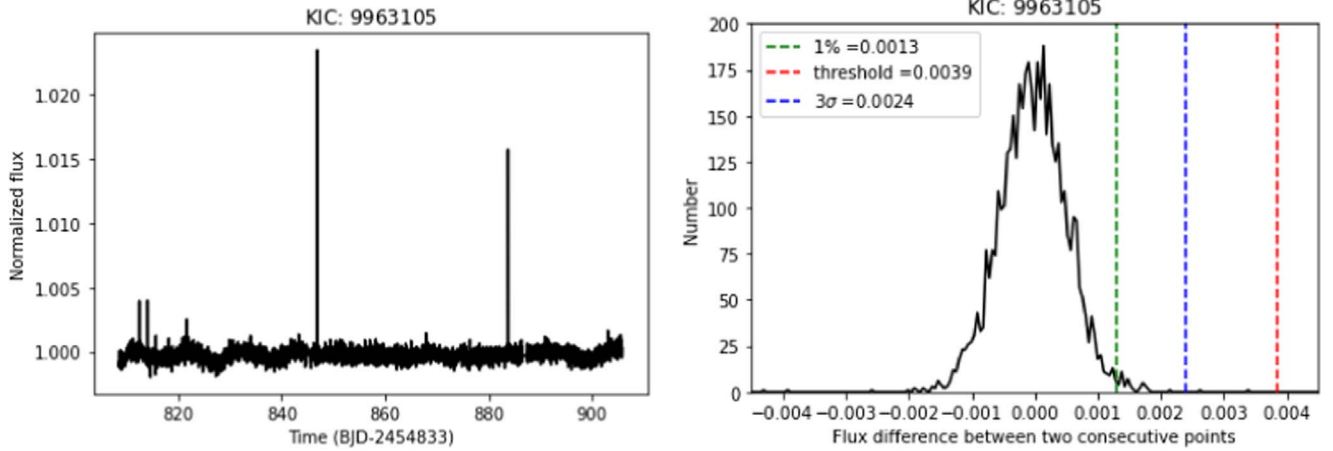


Figure 1. Illustrations of flare detection method used by Shibayama et al. (2013). (a) The light curve of KIC 9963105. (b) The distribution of brightness variation between each pair of adjacent data points in the light curves of KIC 9963105. The green vertical line represents the value of 1% of the total area under the curve, the red vertical line marks the flare detection threshold and the blue vertical line signifies 3σ of the brightness variation distribution.

KIC 9963105. The light curve of KIC 9963105 is plotted in Figure 1(a). Figure 1(b) depicts the distribution of the brightness difference between every two adjacent data points of the KIC 9963105 light curve; 1% of the total area under the distribution curve is represented by the green vertical line. The red vertical line represents the flare detection threshold value, which is equal to three times the 1% value of the area under the distribution curve. The blue vertical line is 3σ of the distribution of the brightness variation. To determine the flare end time, we fit a B-spline curve through three points on the relative flux ($\Delta F/F_{\text{avg}}$) distributed around the flare, one point just before the flare, and the other two points five and eight hours after the flare peak, respectively. Then we subtract the B-spline curve from the relative flux in order to remove long-term brightness variations around the flare (Shibayama et al. 2013). We define the flare end time as the time when the relative flux produced by the subtraction drops below the value of 3σ for the first time. After detecting flare events, conditions are applied to all flare candidates. These conditions are: the flare duration must exceed 0.05 days, corresponding to at least three data points, with two of them after the flare peak, and the flare’s decline phase must be longer than its rising phase (Shibayama et al. 2013). Only flare incidents meeting these criteria were analyzed.

2.2. Energy Calculation

Schaefer et al. (2000) identified nine cases of superflares involving 10^{33} – 10^{38} erg on normal solar-type stars. Their superflare energy estimate has a large uncertainty, e.g., the Groombridge 1830 (HR 4550) total flare energy (in the blue band alone) is 10^{35} erg with an uncertainty of a factor of a few due to having only four points on the light curve.

The possibility that superflares can be explained by magnetic energy stored on the star’s surface was considered by Nogami et al. (2014). Using the Ca II 8542 absorption line, they estimate that the average magnetic field strength (B) of KIC9766237 and KIC9944137 is 1–20 Gauss, and the superflare of these targets has a total energy of 10^{34} erg, under the assumption that the energy released during the flare represents a fraction (f) of the magnetic energy stored around the spot area. Their flare energy (E_{flare}) was calculated as follows

$$E_{\text{flare}} \sim f \frac{B^2}{8\pi} L^3. \quad (3)$$

The length of the magnetic structure causing the flare (L) has been considered to be the same size as the spotted region, i.e., $L = \sqrt{a\pi R_*^2}$ where a is the spot’s area, which yields

$$E_{\text{flare}} \sim f \frac{B^2}{8\pi} (a\pi R_*^2)^{3/2}. \quad (4)$$

Our energy estimation for each flare depends on the star’s luminosity (L_{star}), flare amplitude (f_{amp}) and flare duration (Shibayama et al. 2013; Yang et al. 2017). L_{star} , the amount of energy that the star emits in one second, is proportional to the star’s radius R squared and its surface temperature T_{eff} to the fourth power, and is obtained from the following equation

$$L_{\text{star}} = \sigma_{\text{SB}} T_{\text{eff}}^4 4\pi R^2, \quad (5)$$

where σ_{SB} is the Stefan–Boltzmann constant, and $4\pi R^2$ is the entire surface area of the star. The continuum emission from a WLF is consistent with blackbody radiation at around 9000 K, as suggested by Hawley & Fisher (1992); Kretschmar (2011). Based on Shibayama et al. (2013); Yang et al. (2017); Günther et al. (2020), we set $T_{\text{flare}} = 9000$ K and derive the luminosity

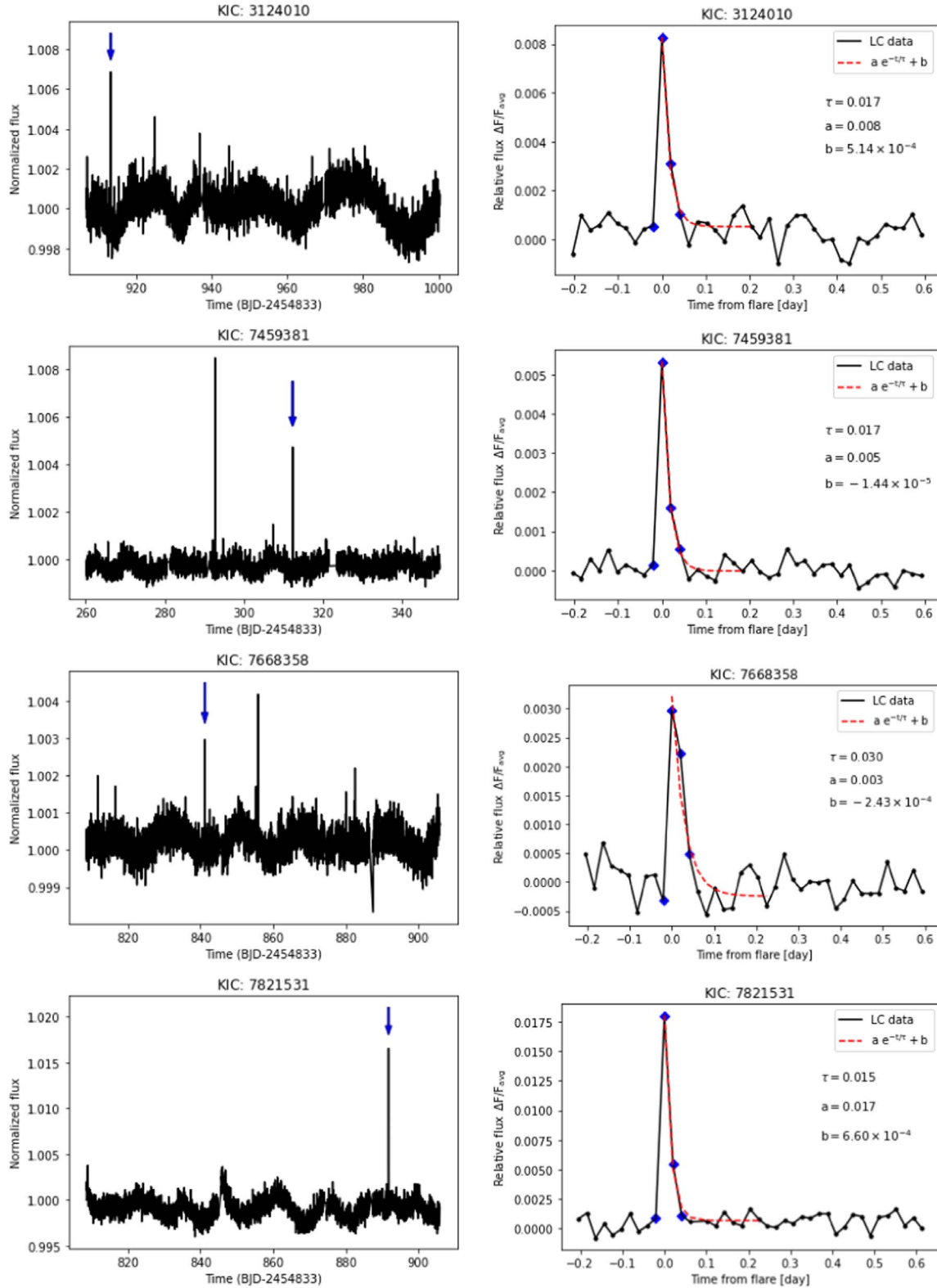


Figure 2. The left panels display the light curves of superflares. The x -axis in the left panels is the time in Barycentric Julian Date (BJD) and the y -axis is the normalized flux. The blue arrows indicate the occurrence of superflares. The right panels show a zoom in time of these superflares. The x -axis in the right panels is the time from the flare peak in day and the y -axis is the relative flux ($\Delta F/F_{avg}$). Each data point for a superflare is represented by a blue square in the right panels. The dashed red curve indicates an exponential fit of the decay phase. τ in the equation refers to the best fit of exponential decay time, a means the final value of the amplitude fit and b represents the fitted relative flux in the quiescent state.

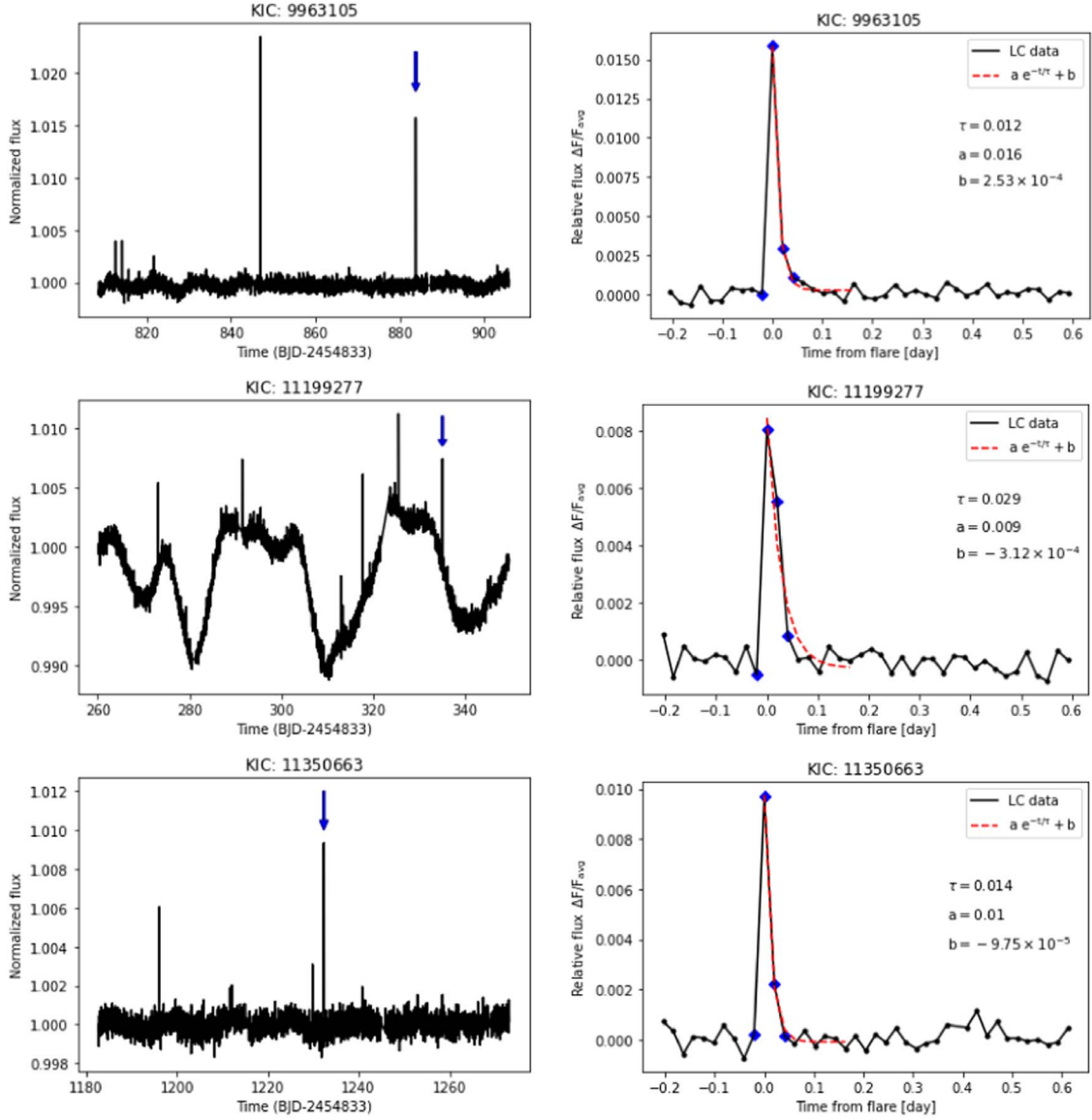


Figure 2. (Continued.)

of a blackbody-emitting star as follows

$$L_{\text{flare}}(t) = \sigma_{\text{SB}} T_{\text{flare}}^4 A_{\text{flare}}, \quad (6)$$

where A_{flare} is the flare's area, as determined by the formula

$$A_{\text{flare}}(t) = f_{\text{amp}}(t) \pi R^2 \frac{\int R_{\lambda} B_{\lambda}(T_{\text{eff}}) d\lambda}{\int R_{\lambda} B_{\lambda}(T_{\text{flare}}) d\lambda}, \quad (7)$$

where f_{amp} represents the flare amplitude for the relative flux and R_{λ} means the Kepler instrument's response function (Caldwell et al. 2010). The Kepler photometer covers various wavelengths, from 420 to 900 nm. The Planck function at a

specific wavelength, denoted by $B_{\lambda}(T)$, is given by

$$B_{\lambda}(T) = \frac{2hc^2/\lambda^5}{e^{hc/\lambda kT} - 1}, \quad (8)$$

where h represents Planck's constant, c the speed of light, T the blackbody temperature and k Boltzmann's constant. By substituting Equation (7) into (6), we calculate the total flare energy by the integral of L_{flare} over the flare duration

$$E_{\text{flare}} = \int_{t_{\text{start}}}^{t_{\text{end}}} L_{\text{flare}}(t) dt. \quad (9)$$

We determine the energy of the flares using the Shibayama et al. (2013) energy estimation method, which assumes

Table 1
Superflares on Slowly Rotating Sun-like Stars

Kepler ID	T_{eff} (K)	$\log g$	Radius (R_{\odot})	$P_{\text{rot}}^{\text{a}}$ (day)	t_{start} (BJD)	t_{end} (BJD)	t_{peak} (BJD)	amp	Flare Duration (day)	τ (day)	Flare Energy (erg)
3124010	5688	4.46	1.01	25.90	913.24	913.30	913.26	0.008	0.061	0.017	4.57×10^{34}
3968932	5716	4.39	0.96	24.56	868.88	868.94	868.90	0.004	0.061	0.026	3.89×10^{34}
7459381	5635	4.27	1.11	26.19	312.31	312.37	312.33	0.005	0.061	0.017	4.89×10^{34}
7668358	5668	4.36	0.98	41.83	841.13	841.19	841.15	0.003	0.061	0.030	1.94×10^{34}
7821531	5681	4.52	0.92	32.66	891.81	891.87	891.83	0.018	0.061	0.015	8.63×10^{34}
9142489	5878	4.51	0.95	25.20	1561.13	1561.19	1561.15	0.004	0.061	0.028	2.61×10^{34}
9528212	5872	4.42	0.97	61.43	1332.34	1332.40	1332.36	0.003	0.061	0.036	2.31×10^{34}
9963105	5751	4.39	1.01	28.09	883.80	883.86	883.82	0.016	0.061	0.012	9.00×10^{34}
10275962	5782	4.51	0.91	26.12	213.21	213.27	213.23	0.007	0.061	0.035	3.71×10^{34}
10275962	5782	4.51	0.91	26.12	599.85	599.91	599.87	0.004	0.061	0.029	2.04×10^{34}
11086906	5758	4.38	1.11	29.18	1206.01	1206.07	1206.03	0.002	0.061	0.018	1.90×10^{34}
11199277	5638	4.49	0.92	29.00	325.43	325.49	325.45	0.008	0.061	0.029	3.72×10^{34}
11350663	5966	4.49	0.96	36.92	1232.31	1232.37	1232.33	0.010	0.061	0.014	5.21×10^{34}
11971032	5942	4.51	0.94	44.00	1231.92	1231.98	1231.94	0.006	0.061	0.030	3.80×10^{34}

Note.

^a Rotation period from McQuillan et al. (2014).

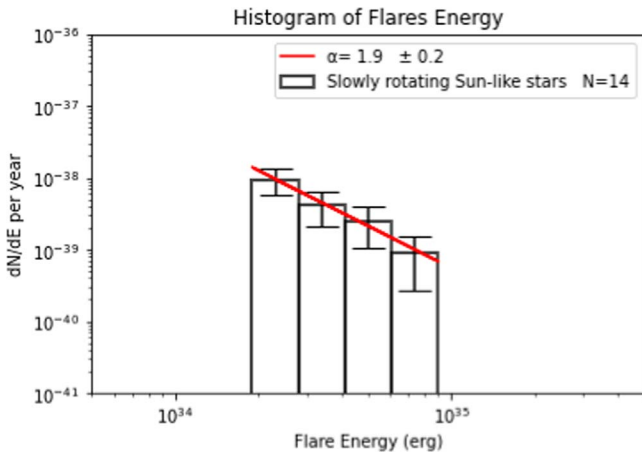


Figure 3. A log-log scale histogram showing the distribution of flare frequency as a function of flare energy of 14 superflares on slowly rotating Sun-like stars. The distribution follows a power-law relation $dN/dE \propto E^{-\alpha}$ where $\alpha = 1.9 \pm 0.2$.

blackbody radiation from both the star and flare, with a fixed flare temperature of 10,000 K, to estimate the quiescent luminosity. We note that the Shibayama et al. (2013) energy estimation can have an error of up to 60% and yet this is more accurate than the one used by Schaefer et al. (2000) and Nogami et al. (2014). To improve the accuracy, Davenport (2016) proposed an alternative method for estimating the quiescent luminosity of each star to determine the actual energy of the flares. They used the Equivalent Duration (ED) parameter, which represents the integral under the flare in fractional flux units, as a relative energy measurement for each flare event without requiring flux calibration of the Kepler light

curves. To calculate the actual energy of the flares emitted in the Kepler bandpass (erg), the ED values (s) are multiplied by the quiescent luminosity (erg s^{-1}) of the respective star. This approach establishes an absolute scale for the relative flare energies, as the quiescent luminosity is individually estimated for each star.

2.3. Rotational Period Determination

Light curve periods were calculated using the Lomb-Scargle periodogram, a common statistical approach for detecting and characterizing periodic signals in sparsely sampled data. We used an oversampling factor of five (VanderPlas 2018), and employed PDCSAP flux to generate a Lomb-Scargle periodogram for each light curve from Q2 to Q16. Furthermore, the period corresponding to the maximum power of the periodogram was allocated as the rotation period for the Kepler ID in a specific quarter. This value was estimated with an accuracy of a day without the decimal component because fractions of a day would not significantly alter the results, allowing us to automate the selection of the star's rotation period rather than doing this manually. We set 0.5 days for periods shorter than a day and eliminated periods less than 0.1 days. Finally, for each Kepler ID, we chose the most frequent period across all quarters from Q2 to Q16. Following the McQuillan et al. (2014) technique, we required that the period chosen for all quarters be identified in at least two unique segments, with the segment defined as three consecutive Kepler quarters: (Q2, Q3, Q4), (Q5, Q6, Q7), (Q8, Q9, Q10), (Q11, Q12, Q13) and (Q14, Q15, Q16).

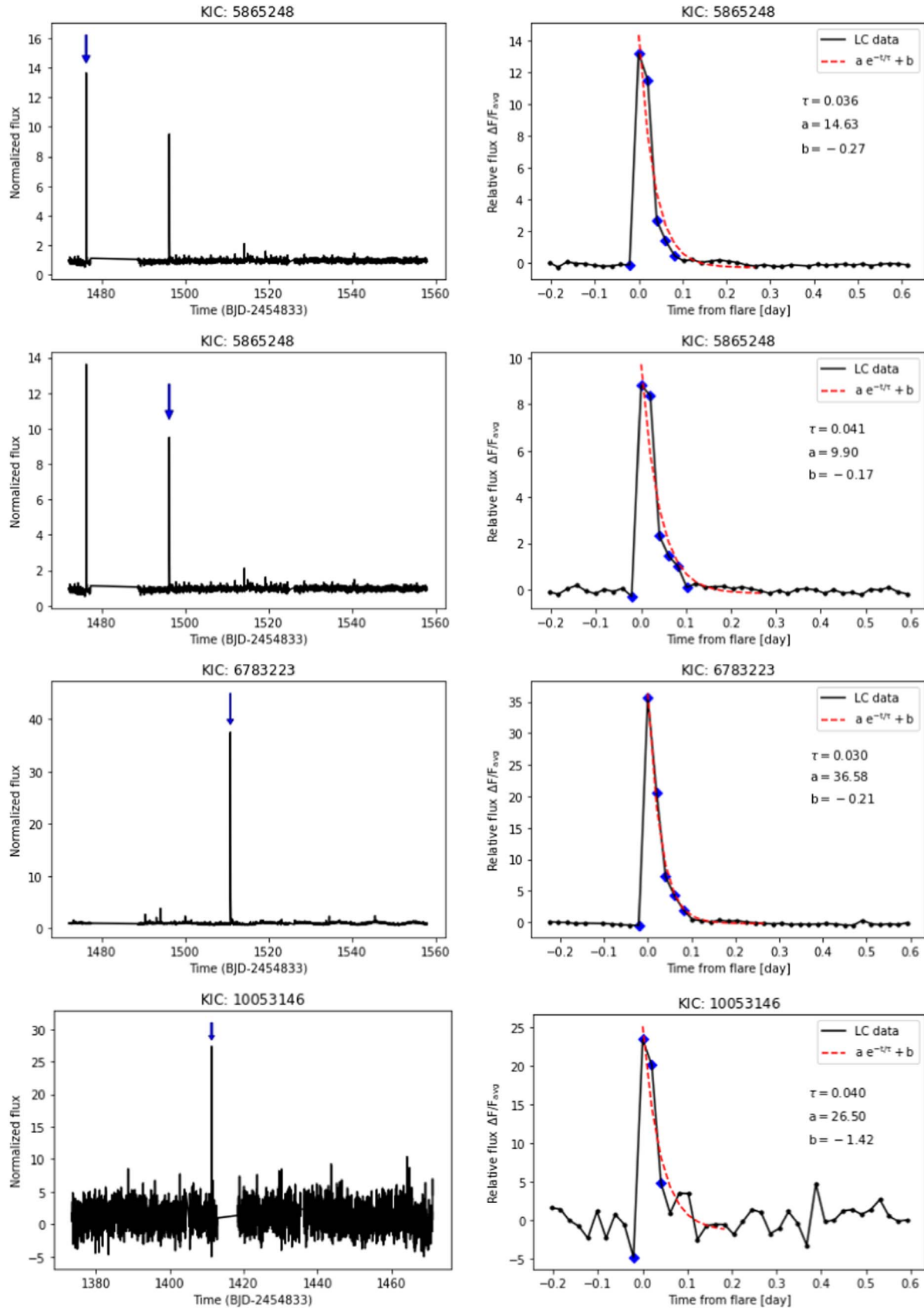


Figure 4. (a) Same as Figure 2 but for large amplitude superflares on G-type main sequence stars.

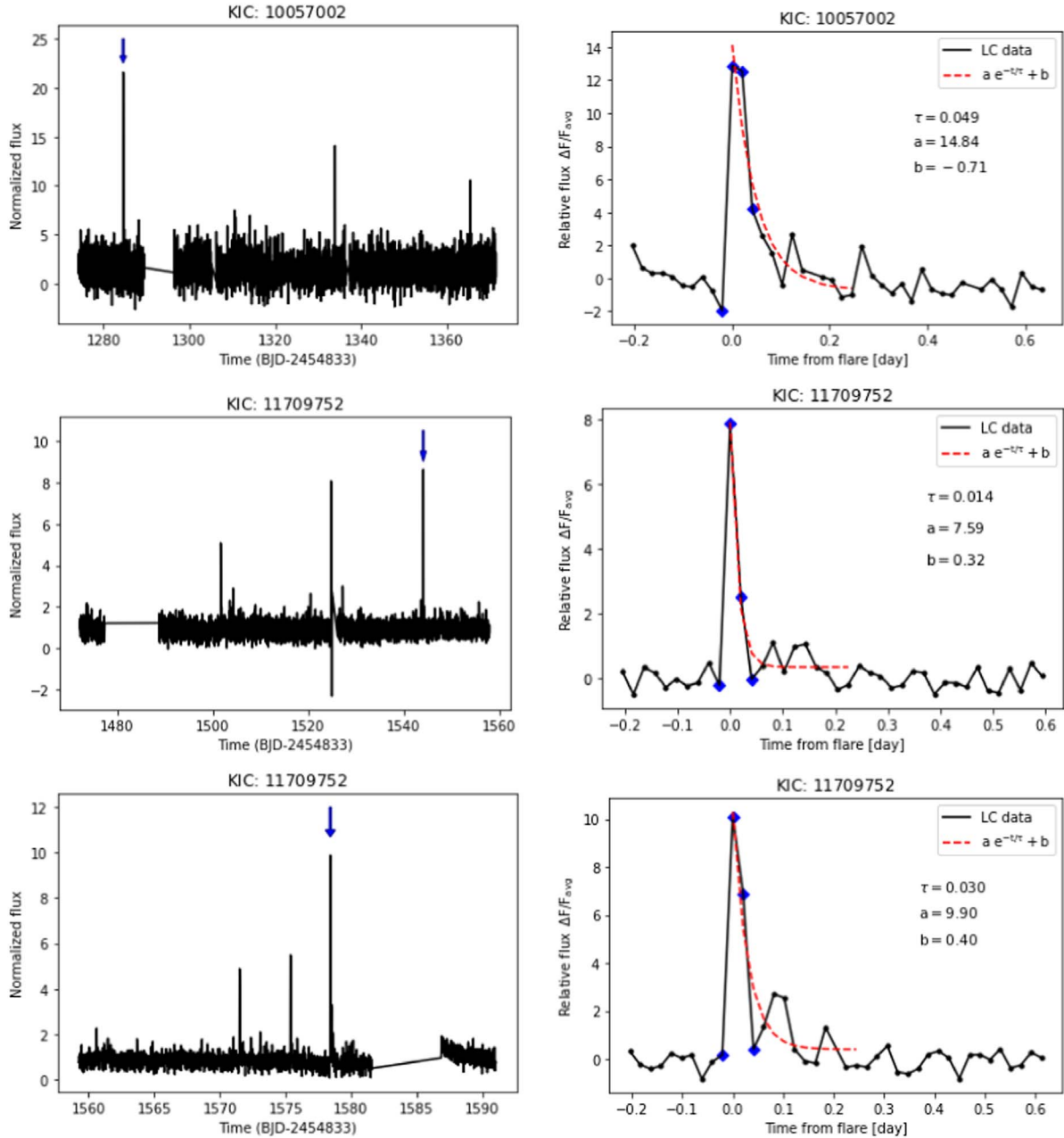


Figure 4. (Continued.)

3. Results

By performing an automated search for superflares on G-type main sequence stars during 1442 days of Kepler observation in all (DR25) long-cadence data from Q0 to Q17, we found 14 superflares on 13 slowly rotating Sun-like stars in each of KIC 3124010, KIC 3968932, KIC 7459381, KIC 7668358, KIC 7821531, KIC 9142489, KIC 9528212, KIC 9963105, KIC 10275962, KIC 11086906, KIC 11199277, KIC

11350663 and KIC 11971032, with surface temperatures of $5600 \text{ K} \leq T_{\text{eff}} < 6000 \text{ K}$, surface gravities of $\log g > 4.0$ and rotational periods P_{rot} ranging between 24.5 and 44 days. Figure 2 depicts seven light curves of these events. The left panels display light curves over 90 days of observation. The blue arrow on the left panel indicates the observed superflare, which met all conditions. The right panels show zoomed in time light curves of superflares. The blue squares represent the data points for a superflare. We fitted an exponential decay

Table 2
Large Amplitude Superflares on G-type Main Sequence Stars

Kepler ID	T_{eff} (K)	$\log g$	Radius (R_{\odot})	$P_{\text{rot}}^{\text{a}}$ (day)	t_{start} (BJD)	t_{end} (BJD)	t_{peak} (BJD)	amp	Flare Duration (day)	τ (day)	Flare Energy (erg)
5865248	5780	4.44	1	NA	1476.22	1476.33	1476.24	13.16	0.102	0.036	7.29×10^{37}
5865248	5780	4.44	1	NA	1496.09	1496.21	1496.11	8.78	0.123	0.041	9.56×10^{37}
5865248	5780	4.44	1	NA	1561.78	1561.86	1561.80	8.14	0.082	0.034	6.75×10^{37}
6783223	5780	4.44	1	NA	1510.76	1510.86	1510.78	35.60	0.102	0.030	8.6×10^{37}
7505473	5780	4.44	1	NA	1385.81	1385.95	1385.85	4.05	0.143	0.058	1.67×10^{36}
10053146	5780	4.44	1	NA	1411.27	1411.33	1411.29	22.75	0.061	0.040	1.42×10^{38}
10057002	5780	4.44	1	NA	1284.52	1284.58	1284.54	12.03	0.061	0.049	6.24×10^{37}
11709752	5780	4.44	1	0.5	1501.56	1501.62	1501.58	4.21	0.061	0.031	2.85×10^{37}
11709752	5780	4.44	1	0.5	1544.06	1544.13	1544.08	7.65	0.061	0.014	2.85×10^{37}
11709752	5780	4.44	1	0.5	1571.49	1571.55	1571.51	4.48	0.061	0.033	3.94×10^{37}
11709752	5780	4.44	1	0.5	1575.35	1575.43	1575.37	5.11	0.082	0.046	5.44×10^{37}
11709752	5780	4.44	1	0.5	1578.39	1578.45	1578.41	9.40	0.061	0.030	3.94×10^{37}

Note.

^a Rotation period from Althukair & Tsiklauri (2023).

function to the flare light curve to characterize the flares, signified by a red dashed curve. This exponential decay function is expressed as

$$f(t) = a e^{-t/\tau} + b, \quad (10)$$

where $f(t)$ is the relative flux as a function of time, a is the flare peak height, which is approximately equal to the relative flux at the flare peak, b is the relative flux in the quiescent state and τ is the decay time of the flare, which is the time at which the relative flux decreases to $1/e \simeq 0.3679$ of its initial value. The values of τ , a and b of the exponential decay function for each flare are shown in the right panel. Flare parameters and their durations, amplitudes, energies and τ values are listed in Table 1. The rotation periods for these slowly rotating Sun-like stars were taken from McQuillan et al. (2014). Their flare energies range from $(1.9\text{--}9.0) \times 10^{34}$ erg. The flare amplitudes of the slowly rotating Sun-like stars are relatively small, ranging between 0.002 and 0.018. We also find that the durations of flares in all of these cases are the same, 0.061 days. This is probably due to the fact that flare durations of all small amplitude superflares are two data points in time or *less*. Therefore, because one of the flare detection conditions in our code is that there must be at least two data points between the flare's peak and the end, cases with flare duration less than two points were not detected, and we ended up with the same duration superflares with the two data points. Because it appears that there are no small amplitude superflares with duration *greater* than two data points, all flare durations end up the same. This selection effect is because we use long cadence light curve data, which has a 29.4 minute interval between each data point in time. The value of τ varies from 0.012 to 0.036 days.

We calculated the frequency distribution of the 14 superflares on the 13 slowly rotating Sun-like stars and plotted a log

scale histogram presenting this distribution as shown in Figure 3. The x -axis represents the flare's energy, and the y -axis corresponds to the number of superflares per star per year per unit of energy. Therefore, we calculated the weight for each bin using

$$w = \frac{3.16 \times 10^7}{N_{\text{os}} \times D \times E}, \quad (11)$$

where N_{os} is the number of observed stars, D is the duration of the observation period in seconds and E is the superflare energy that belongs to that bin. From the number of stars in Table 3 in our previous work, Althukair & Tsiklauri (2023), we estimated that the number of observed G-type dwarfs with $5600 \text{ K} \leq T_{\text{eff}} < 6000 \text{ K}$ and $P_{\text{rot}} > 10$ days is equal to 19,160 stars. Since this distribution is related to slowly rotating Sun-like stars with P_{rot} between 24.5 and 44 days, we estimated the number of observed stars to be one-third of the original sample, i.e., 5635 stars, given that the average rotation period is 34 days which is almost three times the period of 10 days. We estimated the probability of the occurrence of superflares in slowly rotating Sun-like stars with P_{rot} of 24.5–44 days. We found that the rate of superflare incidence with the energy of 4.54×10^{34} erg is 1.94×10^{-4} flares per year per star, corresponding to a superflare occurring on a star once every 5160 yr. We calculated this value by multiplying the average energy from the x -axis by the average dN/dE from the y -axis, $4.54 \times 10^{34} \times 4.27 \times 10^{-39} = 1.94 \times 10^{-4}$ flares per year per star, and by taking the reciprocal of 1.94×10^{-4} , we get 5160 which gives the number of years in which a flare occurs on a star. The frequency distribution of these 14 superflares follows a power-law relation $dN/dE \propto E^{-\alpha}$ where $\alpha = 1.9 \pm 0.2$. This is consistent with our previous result in Althukair & Tsiklauri (2023) for the

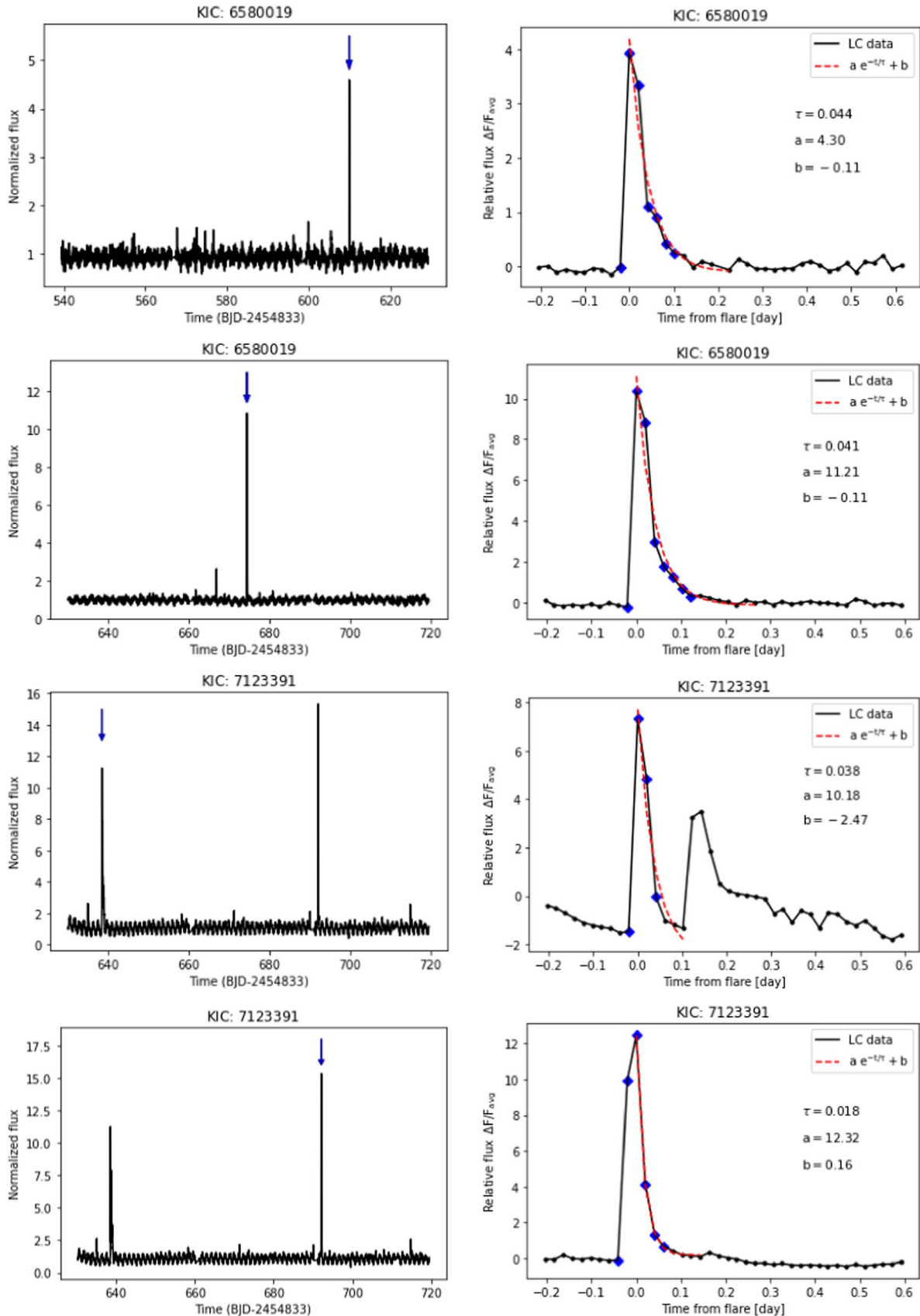


Figure 5. (a) Same as Figures 2 and 4 but for large amplitude superflares on M-type main sequence stars.

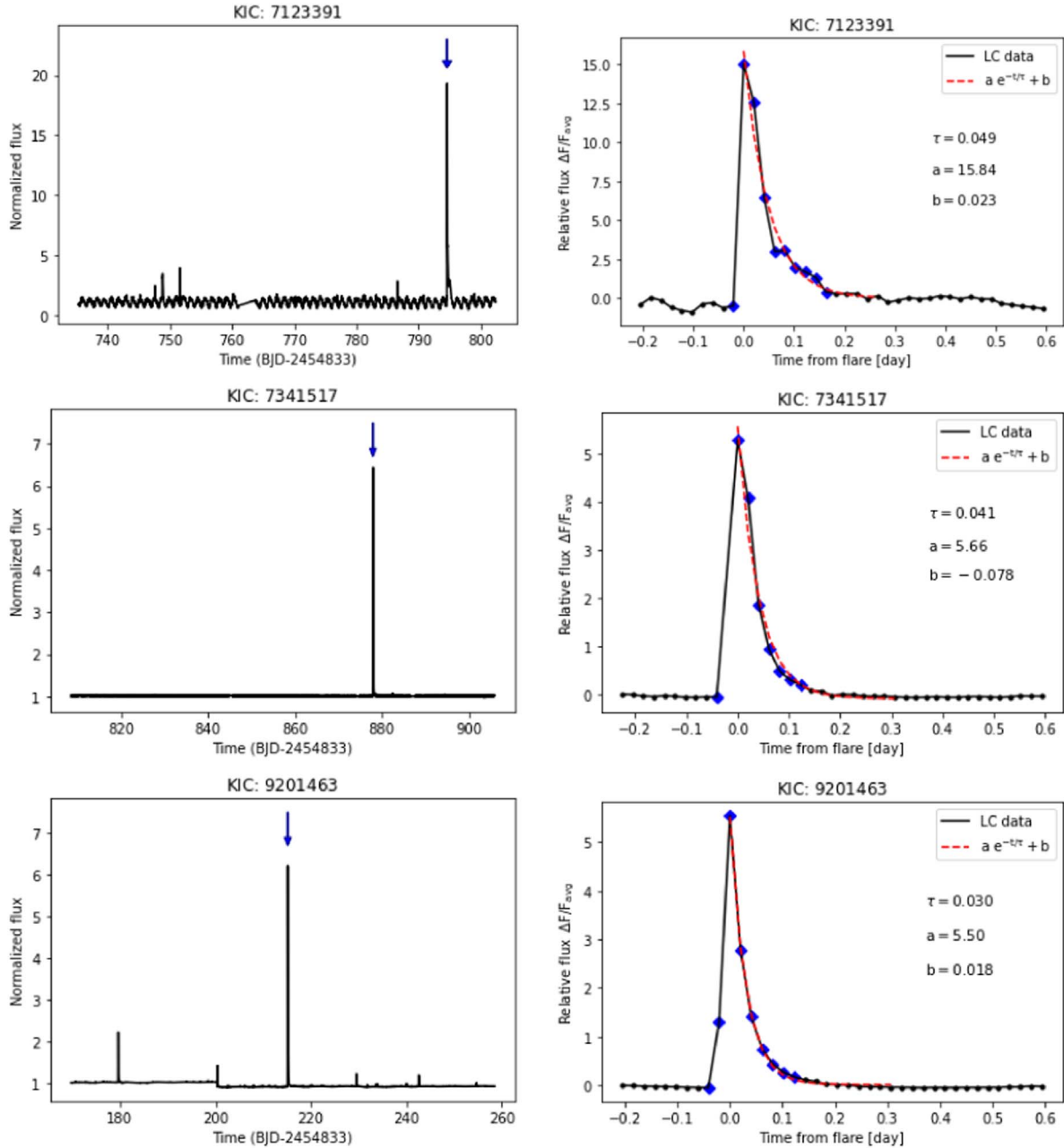


Figure 5. (Continued.)

frequency distribution of slowly rotating G-type dwarfs where $\alpha = 2.0 \pm 0.1$.

In addition to the 14 cases of superflares on slowly rotating Sun-like stars, we detected 12 superflares with a large amplitude on six G-type dwarfs in each of KIC 5865248, KIC 6783223, KIC 7505473, KIC 10053146, KIC 10057002 and KIC 11709752. Figure 4 shows eight light curves of these events, the same as in Figure 2. Table 2 displays the durations,

amplitudes, energies and τ values for these superflares with their parameters. The energies of their flares range from 1.67×10^{36} to 1.42×10^{38} erg. The rotation period of KIC 1170952 was obtained by this work. As for the rotation periods for the other five stars, no such data are available. Even applying the method described in Paper I does not allow period determination in these five cases. According to Yang et al. (2017), there are three possible reasons: (i) due to the

Table 3
Large Amplitude Superflares on M-type Main Sequence Stars

Kepler ID	T_{eff} (K)	log g	Radius (R_{\odot})	P_{rot} (day)	t_{start} (BJD)	t_{end} (BJD)	t_{peak} (BJD)	amp	Flare Duration (day)	τ (day)	Flare Energy (erg)
6580019	2661	5.28	0.12	NA	609.97	610.09	609.99	3.91	0.123	0.044	7.04×10^{33}
6580019	2661	5.28	0.12	NA	674.45	674.60	674.47	10.30	0.143	0.041	1.25×10^{34}
7123391	3326	5.12	0.19	NA	638.53	638.59	638.55	8.07	0.061	0.038	4.76×10^{34}
7123391	3326	5.12	0.19	NA	692.09	692.19	692.13	12.38	0.102	0.018	1.23×10^{35}
7123391	3326	5.12	0.19	NA	794.54	794.72	794.56	15.14	0.184	0.049	1.59×10^{35}
7341517	2661	5.28	0.12	NA	877.95	878.12	877.99	5.27	0.163	0.041	4.82×10^{33}
9201463	3319	5.14	0.18	NA	215.11	215.27	215.15	5.51	0.163	0.030	3.16×10^{33}

inclination angle and low activity level, the light curve has a small amplitude at the accuracy level of Kepler; (ii) fast-rotating stars have spots at the poles (Schüssler & Solanki 1992), making it hard to detect light variation through rotation; and (iii) the rotation period is longer than 90 days (a quarter), making it difficult (or impossible) to detect them in the frequency spectrum of the star. The flare amplitudes for these cases range between 4.05 and 35.60. These flares tend to last longer than flares with smaller amplitudes on slowly rotating Sun-like stars as their durations vary between 0.061 and 0.143 days. The τ values of flares exhibiting large amplitude on G-type main sequence stars are observed to be higher than those of flares occurring on slowly rotating Sun-like stars, as their values range between 0.014 and 0.058 days.

For stars of other spectral classes, no significant flares with large amplitudes were detected on main sequence stars of types A, F or K. Only M-type main sequence stars manifested seven superflares with large amplitude on each of KIC 6580019, KIC 7123391, KIC 7341517 and KIC 9201463. Similar to Figures 2 and 4, 5 displays the seven light curves for these events. The parameters of these superflares, including their durations, amplitudes, energies and τ values, are listed in Table 3. These flares have an energy between 3.16×10^{33} and 1.59×10^{35} erg, amplitude ranges between 3.91 and 15.14 and their duration lasts between 0.018 and 0.044 day. τ values for superflares with large amplitude on M-type main sequence stars vary from 0.030 to 0.049 days.

We examined whether there is a dependence between τ versus flare amplitude (f_{amp}) and τ versus flare energy (E_{flare}). Therefore, we graphically display six panels in Figure 6 showing the relationship between τ and the amplitude of flares and τ and the energy of flares in slowly-rotating Sun-like stars in Figure 6(a), (b), G-type stars in 6(c), (d) and M-type stars in 6(e), (f). In Figure 6(a) for slowly rotating Sun-like stars, we find that for small amplitude, τ is large, and when the amplitude is large, τ is consistently small in the range considered. The same applies to the relation between τ and energy in Figure 6(b); we see that large τ values correspond to small energies and small values of τ correspond

to large energies considered. On the contrary, there is no clear relation between τ versus f_{amp} and τ versus E_{flare} in G-type and M-type main sequence stars in Figure 6(c)–(f). However, as mentioned in the Introduction, according to Maehara et al. (2015), the duration of superflares, τ , scales as the flare energy, E , according to $\tau \propto E^{0.39 \pm 0.03}$. Similarly, Tu et al. (2020) found that $T_{\text{duration}} \propto E^{0.42 \pm 0.01}$. It broadly follows, from the simple reconnection scaling arguments, that $\tau \propto E^{1/3}$. We believe that we could not deduce such scaling because of the small number of data points in Figure 6. We tried various functions for fit using Python's *curve_fit* and Excel's *trendline*, referred to as a line of best fit, to visualize the general trend for the data. We could not find any reliable, functional fit dependence between those parameters because the *coefficient of determination*, R^2 , which is a measure of how well the data fit the regression model, is less than 0.5 for all those cases in Figure 6(a to f). Hence any attempted fit has been unreliable, as only a fit with $R^2 > 0.5$ can be deemed acceptable. To determine the extent to which the two variables, τ and flare amplitude, as well as τ and flare energy, are correlated, we calculated the *Pearson Correlation Coefficient* (r), which measures the strength and direction of the relationship between two variables, using IDL's built-in function CORRELATE(X, Y) and Python's function *scipy.stats.pearsonr*. Both IDL and Python gave the same values. The values for the Pearson correlation coefficient (r) between two data sets are listed in Table 4. We note that for the slowly rotating Sun-like stars data sets, $r = -0.592$ and $r = -0.691$ for τ versus f_{amp} and τ versus E_{flare} respectively, which suggest a noticeable negative correlation between the variables. For the remaining four cases, these r values are close to zero, which indicates a weak or nonexistent correlation between the two variables. In general, r varies from -1 to 1 . The extreme cases of $r = \pm 1$ mean that there is a clear linear correlation/anticorrelation. $r = 0$ indicates that there is no linear relation between the variables.

In the context of explaining the absence of large-amplitude flares detected in A-, F- and K-type main sequence stars, while they are only detected in G-type and M-type stars we would

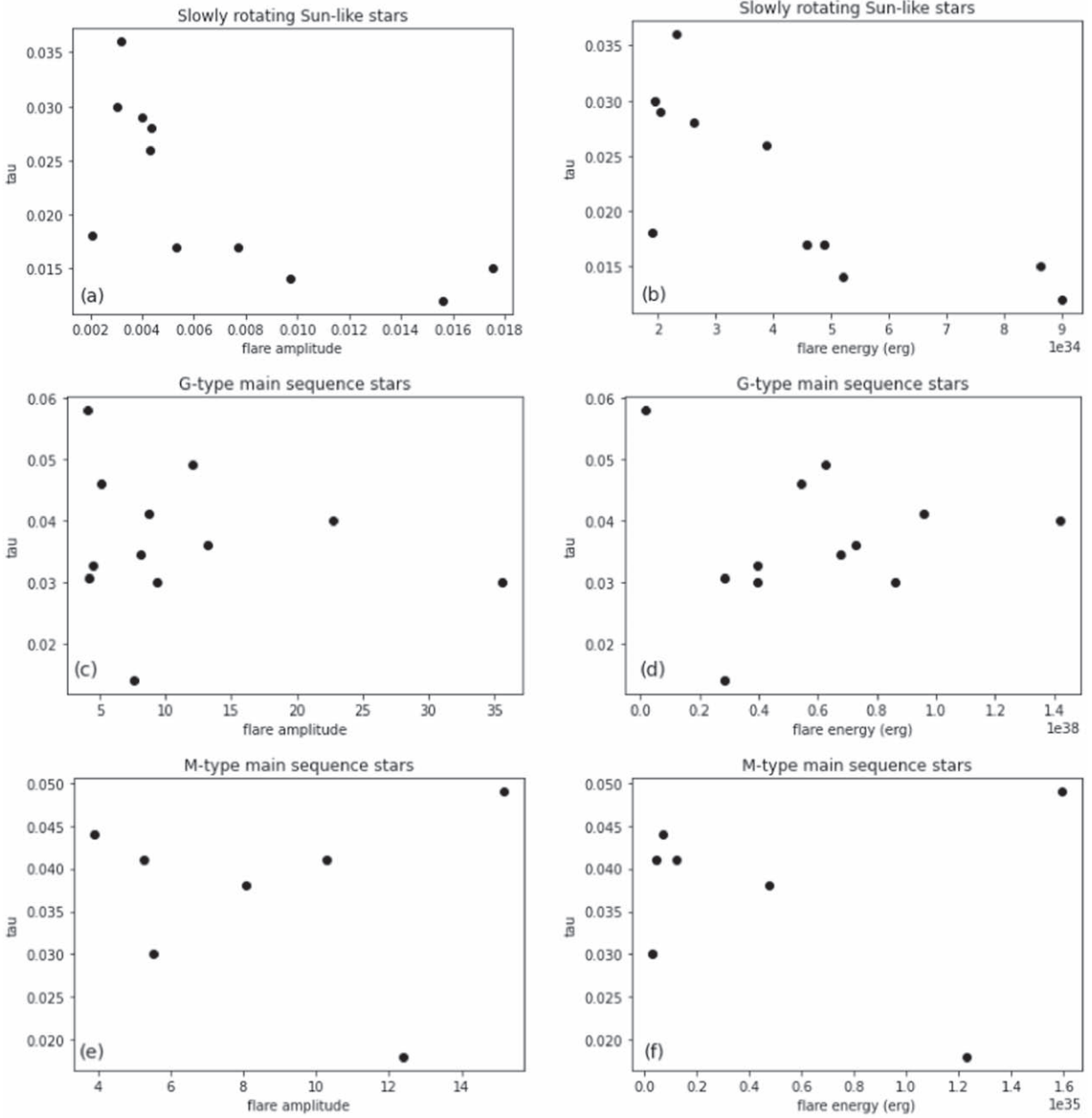


Figure 6. The left panels display a scatter plot showing the relation between τ values on the y-axis with the flare amplitude f_{amp} on the x-axis, while the right panels display a scatter plot showing the relation between τ values on the y-axis with the flare energy E_{flare} on the x-axis. For flares on slowly rotating Sun-like stars, (a) demonstrates that τ values are large for low flare amplitudes but consistently small for high flare amplitudes. Likewise, (b) affirms that high τ values correspond to low flare energies, whereas low τ values correspond to high flare energies. For large amplitude superflares on G-type dwarfs (c,d) and M-type dwarfs (e,f), τ has no clear connection to the f_{amp} or E_{flare} .

like to remark the following. Using the Kepler space telescope, Chang et al. (2018) studied the light curves of the M dwarfs. They found a number of flare events with the peak flux increasing as $\Delta F/F \geq 1$. Magnetic fields of the M dwarfs are generated by a turbulent magnetic dynamo mechanism. This is due to their deep convective zones, and this leads to very

powerful flares, compared to G-type stars (Davenport et al. 2014). As for G-type stars, the detection of strength of flares in such stars has been known for some time starting from Maehara et al. (2012). Therefore it is not entirely surprising that that we detected large-amplitude flares in G- and M-type stars. As for A-, F- and K-type stars, we remark that according to

Table 4The Pearson Correlation Coefficient between τ vs. f_{amp} and τ vs. E_{flare}

Sample	τ versus f_{amp}	τ versus E_{flare}
Slowly rotating Sun like stars	-0.592	-0.691
G-type large amplitude flares	-0.149	0.141
M-type large amplitude flares	-0.046	-0.098

Pedersen et al. (2016) for the flare generation, stars must have: either a deep outer convection zone for F5-type and perhaps later-types; or strong, radiatively driven winds for B5-type and earlier types; or strong large-scale magnetic fields for A and B-type stars. Pedersen et al. (2016) and earlier works suggest that normal A-type stars have no such features and thus should not flare. However, flares and superflares have previously been detected on such stars according to Bai & Esamdin (2020) and references therein. The situation with K-type stars is somewhat a “gray area.” Stars less massive and cooler than our Sun are K dwarfs; and even fainter and cooler stars are the red-colored M dwarfs. Thus K dwarfs are probably a borderline case where large-amplitude flares can occur.

4. Conclusions

Using our Python script on long cadence data from DR25, we searched for superflares on main sequence stars of types A, F, G, K and M based on the entire Kepler data following the method of Maehara et al. (2012); Shibayama et al. (2013). The Kepler targets’ parameters were retrieved from the Kepler Stellar interactive table in the NASA Exoplanet Archive. Using these data, we detected 14 superflares on 13 Sun-like stars with surface temperatures of $5600 \text{ K} \leq T_{\text{eff}} < 6000 \text{ K}$, with P_{rot} ranging from 24.5 to 44 days. In addition, we found 12 and seven cases of large amplitude superflares on six and four main sequence G- and M-type stars, respectively. Main sequence stars of other spectral types A, F and K showed no signs of large-amplitude superflares. To characterize the flares, we fit an exponential decay function to the flare light curve given by $f(t) = a e^{-t/\tau} + b$. We study the relation between the decay time of the flare after its peak τ versus f_{amp} and τ versus E_{flare} . For slowly rotating Sun-like stars, we find that τ is large for small flare amplitudes and τ is small for large flare amplitudes considered. Similarly, we find that large τ values correspond to small flare energies and small τ values correspond to high flare energies considered. However, for the main sequence stars with G- and M-types, τ has no apparent relation to the f_{amp} or E_{flare} . We experimented with several different fit functions between τ versus f_{amp} and τ versus E_{flare} to better see the underlying pattern in the data. Since the R^2 is less than 0.5 in these cases, we could not identify a reliable fit functional dependence between these parameters.

In conclusion, we believe that:

(i) the thirteen peculiar Kepler IDs are Sun-like, slowly rotating with rotation periods of 24.5–44 days and yet can produce a superflare with energies in the range of $(2-9) \times 10^{34}$ erg;

(ii) we found six G-type and four M-type Kepler IDs with exceptionally large amplitude superflares, with the relative flux in the range $\Delta F/F_{\text{avg}} = 4-35$.

These cases that we found defy our current understanding of stars and hence are worthy of further investigation.

Acknowledgments

Some of the data presented in this paper were obtained from the Mikulski Archive for Space Telescopes (MAST). STScI is operated by the Association of Universities for Research in Astronomy, Inc., under NASA contract NAS5-26555. Support for MAST for non-HST data is provided by the NASA Office of Space Science via grant NNX13AC07G and by other grants and contracts.

Authors would like to thank Deborah Kenny of STScI for kind assistance in obtaining the data, and Cozmin Timis and Alex Owen of Queen Mary University of London for the assistance in data handling at the Astronomy Unit.

A. K. Althukair wishes to thank Princess Nourah Bint Abdulrahman University, Riyadh, Saudi Arabia and the Royal Embassy of Saudi Arabia Cultural Bureau in London, UK for the financial support of her PhD scholarship, held at Queen Mary University of London.

Authors would like to thank an anonymous referee whose comments greatly improved this manuscript.

Data Availability

All data used in this study were generated by our bespoke Python script that can be found at <https://github.com/althukair/AFD> under the filename AFD.py and other files in the same GitHub repository. The data underlying this article were accessed from Mikulski Archive for Space Telescopes (MAST) <https://mast.stsci.edu/portal/Mashup/Clients/Mast/Portal.html>. The long-cadence Kepler light curves analyzed in this paper can be accessed via MAST STScI (2016). The Kepler Stellar parameters table for all targets can be found at Mission (2019). The derived data generated in this research will be shared on reasonable request to the corresponding author.

ORCID iDs

A. K. Althukair  <https://orcid.org/0000-0003-4075-4440>
D. Tsiklauri  <https://orcid.org/0000-0001-9180-4773>

References

Althukair, A. K., & Tsiklauri, D. 2023, *RAA*, 23, 085017
Bai, J.-Y., & Esamdin, A. 2020, *ApJ*, 905, 110

- Caldwell, D. A., Van Cleve, J. E., Jenkins, J. M., et al. 2010, *Proc. SPIE*, **7731**, 773117
- Chang, H.-Y., Lin, C.-L., Ip, W.-H., et al. 2018, *ApJ*, **867**, 78
- Chen, H., Tian, H., Li, H., et al. 2022, *ApJ*, **933**, 92
- Davenport, J. R. A. 2016, *ApJ*, **829**, 23
- Davenport, J. R. A., Hawley, S. L., Hebb, L., et al. 2014, *ApJ*, **797**, 122
- Gao, D.-Y., Liu, H.-G., Yang, M., & Zhou, J.-L. 2022, *AJ*, **164**, 213
- Günther, M. N., Zhan, Z., Seager, S., et al. 2020, *AJ*, **159**, 60
- Hawley, S. L., & Fisher, G. H. 1992, *ApJS*, **78**, 565
- He, H., Wang, H., & Yun, D. 2015, *ApJS*, **221**, 18
- He, H., Wang, H., Zhang, M., et al. 2018, *ApJS*, **236**, 7
- Ilin, E., Poppenhaeger, K., Schmidt, S. J., et al. 2021, *MNRAS*, **507**, 1723
- Jackman, J. A. G., Wheatley, P. J., Bayliss, D., et al. 2019, *MNRAS*, **485**, L136
- Karak, B. B., Käpylä, P. J., Käpylä, M. J., et al. 2015, *A&A*, **576**, A26
- Karak, B. B., Tomar, A., & Vashishth, V. 2020, *MNRAS*, **491**, 3155
- Katsova, M. M., Kitchatinov, L. L., Livshits, M. A., et al. 2018, *ARep*, **62**, 72
- Kitchatinov, L. L., Mordvinov, A. V., & Nepomnyashchikh, A. A. 2018, *A&A*, **615**, A38
- Kitchatinov, L. L., & Olemskoy, S. 2016, *MNRAS*, **459**, 4353
- Kretschmar, M. 2011, *A&A*, **530**, A84
- Lu, H.-p., Zhang, L.-y., Shi, J., et al. 2019, *ApJS*, **243**, 28
- Maehara, H., Shibayama, T., Notsu, S., et al. 2012, *Natur*, **485**, 478
- Maehara, H., Shibayama, T., Notsu, Y., et al. 2015, *EP&S*, **67**, 59
- Masuda, S., Kosugi, T., Hara, H., Tsuneta, S., & Ogawara, Y. 1994, *Natur*, **371**, 495
- McIntosh, P. S., & Donnelly, R. F. 1972, *SoPh*, **23**, 444
- McQuillan, A., Mazeh, T., & Aigrain, S. 2014, *ApJS*, **211**, 24
- Mission Kepler 2019, Kepler Stellar Properties Table, IPAC
- Neidig, D. F. 1989, *SoPh*, **121**, 261
- Neidig, D. F., & Cliver, E. W. 1983, *SoPh*, **88**, 275
- Nogami, D., Notsu, Y., Honda, S., et al. 2014, *PASJ*, **66**, L4
- Pedersen, M. G., Antoci, V., Korhonen, H., et al. 2016, *MNRAS*, **466**, 3060
- Schaefer, B. E., King, J. R., & Deliyannis, C. P. 2000, *ApJ*, **529**, 1026
- Schmidt, S. J., Shappee, B. J., Gagné, J., et al. 2016, *ApJL*, **828**, L22
- Schüssler, M., & Solanki, S. 1992, *A&A*, **264**, L13
- Shibata, K., Masuda, S., Shimojo, M., et al. 1995, *ApJ*, **451**, L83
- Shibayama, T., Maehara, H., Notsu, S., et al. 2013, *ApJS*, **209**, 5
- STScI 2016, Kepler LC, Q0-Q17, STScI/MAST
- Tu, Z.-L., Yang, M., Zhang, Z. J., & Wang, F. Y. 2020, *ApJ*, **890**, 46
- Van Doorsselaere, T., Shariati, H., & Debosscher, J. 2017, *ApJS*, **232**, 26
- VanderPlas, J. T. 2018, *ApJS*, **236**, 16
- Worden, S. 1983, Byrne PB, Rodono M. (Holland: D. Reidel Publ. Co.), 207
- Wu, C.-J., Ip, W.-H., & Huang, L.-C. 2015, *ApJ*, **798**, 92
- Wu, Y., Chen, H., Tian, H., et al. 2022, *ApJ*, **928**, 180
- Yang, H., & Liu, J. 2019, *ApJS*, **241**, 29
- Yang, H., Liu, J., Gao, Q., et al. 2017, *ApJ*, **849**, 36
- Yang, Z., Zhang, L., Meng, G., et al. 2023, *A&A*, **669**, A15